Journal of Solid State Chemistry 183 (2010) 1863–1871

Contents lists available at ScienceDirect

Journal of Solid State Chemistry

journal homepage: www.elsevier.com/locate/jssc

Magneto-thermal and dielectric properties of biferroic $YCrO_3$ prepared by combustion synthesis

A. Durán [a,*], A.M. Arévalo-López [b], E. Castillo-Martínez [b], M. García-Guaderrama [c], E. Moran [b], M.P. Cruz [a], F. Fernández [d], M.A. Alario-Franco [b]

[a] Universidad Nacional Autónoma de México, Centro de Nanociencias y Nanotecnología, Apartado Postal 2681, C.P. 22800, Ensenada, B.C., México
[b] Departamento de Química Inorgánica y Laboratorio Complutense de Altas Presiones, Facultad de Química, Universidad Complutense de Madrid, E.U., 28040 Madrid, Spain
[c] Centro de Investigación en Materiales DIP-CUCEI, Universidad de Guadalajara. Av. Revolución 1500, Col. Olímpica, Guadalajara, México
[d] Universidad Politécnica de Madrid, E.U. Ingeniería Técnica Industrial, Ronda de Valencia, 3, E-28012 Madrid, Spain

ARTICLE INFO

Article history:
Received 21 April 2010
Received in revised form
2 June 2010
Accepted 4 June 2010
Available online 16 June 2010

Keywords:
Multiferroics
Structure
Magnetism
Specific heat
Dielectric properties

ABSTRACT

Microstructural, magnetothermal and dielectric properties of $YCrO_3$ powders prepared by combustion and solid state methods have been studied by a combination of XRD, specific heat, magnetization and permittivity measurements. The TEM and XRD characterization confirm that the combustion powders are amorphous plate-like agglomerates of nano-sized crystalline particles. A more uniform grain size along with an increase of the relative density is observed by SEM in the sintered samples prepared by combustion route with respect to those produced by solid state reaction. Similar to the material obtained through solid state synthesis, the material prepared by the combustion method also shows spin canted antiferromagnetic ordering of Cr^{+3} ($S=3/2$) at $\sim$140 K, which is shown by magnetization as well as λ-type anomaly in the total specific heat. Furthermore, the magnetic contribution to the total specific heat reveals spin fluctuations above T_N and a spin reorientation transition at about 60 K. Both $YCrO_3$ compounds show a diffuse phase transition at about 450 K, typical of a relaxor ferroelectric, which is characterized by a broad peak in the real part of the dielectric permittivity as a function of temperature, with the peak decreasing in magnitude and shifting to higher temperature as the frequency increases. The relaxor dipoles are due to the local non-centrosymmetric structure. Furthermore, the high loss tangent in a broad range of temperature as well as conductivity analysis indicates a hopping mechanism for the electronic conductivity as we believe it is a consequence of the outer d^3-shell, which have detrimental effects on the polarization and the pooling process in the $YCrO_3$ bulk material. The more uniform particle size and higher density material synthesized through the combustion process leads to an improvement in the dielectric Properties.

© 2010 Elsevier Inc. All rights reserved.

1. Introduction

Orthochromites of formula $RCrO_3$ (R=Y and rare earth) are an interesting family of compounds showing a large variety of physical and chemical properties depending of the rare earth ion lying in the *A*-site of the perovskite structure [1]. In the past decades many investigations were focused in their magnetic and electronic behavior at low temperature. In addition, its high chemical stability at high temperature has been of great interest as they can find applications in high-temperature electrodes and thermoelectric materials [2–4]. Furthermore, in recent years this group of compounds has received wide attention because of the possibility of combining ferroelectric and ferromagnetic properties in the same volume of the same compound [5,6]. One of these compounds is the $YCrO_3$ perovskite, for which experimental evidences recently showed a biferroic behavior [5]. The crystal structure has been indexed as an orthorhombic cell with *Pbnm* space group in a large number of works [1,7]. This fact is intriguing since the *Pbnm* space group is centrosymmetric and it does not account for the biferroic behavior. The off-centering distortion remains a puzzle, for instance, Ramesha et al. [8] have proposed the concept of 'local noncentrosymmetry' to account for the observed permittivity peak and the small value of the polarization reported by Serrao et al. [5]. There, the dielectric behavior and the poor hysteresis loops seem to indicate that the electric transport are very far from being optimized in this material. In many cases, the dielectric response is connected with the synthesis process. $YCrO_3$ shows poor sinterability and it is quite difficult to obtain high density in the bulk material under normal conditions.

It is known that the conventional solid state synthesis method depends on the ions diffusion through the reactants and, in order

* Corresponding author.
E-mail address: dural@cnyn.unam.mx (A. Durán).

0022-4596/$ - see front matter © 2010 Elsevier Inc. All rights reserved.
doi:10.1016/j.jssc.2010.06.001

to obtain uniform products it requires repeated grinding with subsequent long firing cycles at high temperatures. This ceramic route provides poor control of the morphology and a broad dispersion in particle size leading to undesirable features, such as phase and stoichiometry inhomogeneities and the concomitant dispersion of properties in the final products. Nowadays a variety of new methods is being used in order to get the optimal final reaction products. Some of the chemical methods of synthesis of oxides that are especially noteworthy are as follows: the precursor method, coprecipitation and soft chemistry route, sol–gel, intercalation and ion exchange method, topochemical route and one of them that in recent years has attracted the attention is the self-propagation high temperature reaction, also called 'combustion method' [10]. The latter method provides a good control of the stoichiometry and structure, homogeneous microstructural products and also is cheap and easy to use in the laboratory. Many of these methods often also require final thermal treatments to achieve the crystallization of the desired products. Combustion synthesis, also known as self-propagation high temperature synthesis, is a versatile alternative route that in recent years has been used in different areas of the materials science of technological interest. Combustion synthesis is far-from-equilibrium processing method which uses highly exothermic ($\Delta H < -170$ kJ/mol) and even explosive reactions to maintain a self-propagation high temperature reaction [9,10]. Once ignited, the reaction propagates as a wave through the raw materials in solution, and losing less heat than it is generated so as not to quench; temperatures up to 3000 K are maintained during the fast reaction period, which in many cases produce amorphous nanoparticles that can crystallize with the help of post thermal treatments. Self-ignition can sometimes be achieved by ball milling which in turn was initially conceived to synthetize nanocrystalline metals/alloys and nanopowders of refractory materials, including borides, nitrides, oxides, intermetallics and ceramic materials [10]. Thus, self-propagation high temperature synthesis offers the possibility to manipulate the structural and microstructural morphology with relatively few calcination steps to obtain a stable stoichiometric ratio and a homogeneous particle size. Nanocrystalline $YCrO_3$ powder has already been synthesized by a combustion technique and magnetization studies on those samples have shown a weak ferromagnetic ordering at $T_N = 140$ K similar to that observed in the bulk material [5]; however, the effect of this synthetic procedure on the dielectric properties of the material was not studied. Here, we have prepared the $YCrO_3$ perovskite by means of two routes of synthesis: combustion method and solid state reaction. We have then investigated the advantages of this technique and the connection between microstructure and the magnetic, thermal and dielectric features in $YCrO_3$.

2. Experimental procedure

Polycrystalline samples were prepared by the conventional solid state reaction and the combustion method. The first samples were synthesized from high purity Y_2O_3 and Cr_2O_3 powders, mixed in a stoichiometric ratio and heated in air at 1200 °C for 15 h in high density Al_2O_3 crucibles. Two subsequent heating at 1350 °C for 15 h with intermediate grindings were enough to attain the single phase. The final powder was compacted into pellets (11 mm × 1.2 mm) at 4 ton and sintered at 1400 °C for 15 h. For the second samples stoichiometric quantities of yttrium nitrate [$Y(NO_3)_3 \cdot 6H_2O$] and chromium nitrate [$Cr(NO_3)_3 \cdot 9H_2O$] were dissolved in 2-metoxiethanol (1 g:10 ml) while stirring and then heated at about 70 °C until the raw nitrates were completely dissolved. The mixed solution was then added to an Al_2O_3 flask and heated at 120 °C. The solvent was continuously evaporated and finally auto-ignited with a rapid evolution of large volumes of gases to produce voluminous powders. The reaction products were fine powders that were subsequently grinded and fired in a two step process: first at a slow heating rate of 1 °C/min to reach 800 °C for 1 h and then heated at the same rate to reach 1100 °C for 6 h. The final products were pressed into pellets (11 mm × 1.2 mm) at 4 tons and sintered at 1400 °C for 12 h.

Simultaneous differential scanning calorimetric (DSC) and thermogravimetric analysis (TGA) were performed in order to determine the subsequent full crystallization of the combustion product. The analysis was carried out in a TA Instrument, Universal Analysis 2000. The specimens were heated in an oxygen flow from 305 to 1273 K at rate of 10 °C/min. X-ray powder diffraction patterns for Rietveld refinement were collected with a Phillips X'Pert PRO ALPHA 1 diffractometer with Cu$K\alpha 1 = 1.54056$ Å radiation and equipped with a Ge (111) monochromator, working on the Bragg–Bentano geometry. Data were collected in the range of $10^\circ < 2\theta < 120^\circ$ with a step size of 0.017° collected for 100 s. The crystalline structure was refined with the program Rietica [11] (Rietveld program for quantitative phase analysis of polycrystalline mixtures with multi-phase capability).

Transmission electron microscopy (TEM) was performed using a JEM 2000-FX TEM operated at 200 keV. An ultrasound bath was used to disperse the nanopowders in *n*-butanol. A drop of this suspension was evaporated into holey carbon coated copper grids.

Magnetization and specific heat were measured using a commercial quantum design SQUID magnetometer and a quantum design physical properties measurement system (PPMS), respectively. DC magnetization was measured with applied magnetic fields of 0.1 and 10 kOe and the magnetization loops were obtained with applied magnetic fields of up to ±5 T. Furthermore, specific heat was measured down to 2 K in zero applied magnetic fields. For dielectric measurements silver electrodes were painted on discs in order to make parallel-plate ceramic capacitors. Capacitance measurements were carried out from room temperature up to ~800 K at different frequency in the range of 10 kHz–1 MHz using an LCR bridge (HP-4284A).

3. Results and discussion

3.1. Powder characterization

Fig. 1 displays simultaneous DSC and TGA thermal analyses of the fine well milled combustion powder. The small anomaly at ~453 K in the DSC curve is assigned to the dehydration of the combustion powder. The broad endothermic peak from 453 to ~613 K in the DSC with an initial weight loss in the TGA of ~3.5% is attributed to the decomposition of weakly coordinated precursors evolving small quantities of gaseous products like CO, CO_2, NO_2, N_2, etc. Further heating shows a continuous decrease in the DSC curve with a minimum at 600 °C accompanied by a weight increase in the TGA signal at the same range of temperature (see arrows in Fig. 1). These are ascribed to the first crystallization of $YCrO_4$ via the absorption of oxygen from the air. According to the literature the first stable crystallization upon heating correspond to the $YCrO_4$ compound which takes place between 773 and 973 K depending of the fuel-type and oxidant-fuel ratio [12–14]. In this case, it is observed that the first crystallization of $YCrO_4$ from the amorphous phase occurs at ~613 K and is completed at ~873 K as can be seen by the weight maximum in the TGA curve. For clarity, the continuous line in the TGA data (black line and arrows in Fig. 1) shows the range where the $YCrO_4$ undergoes the decomposition following the reaction: $YCrO_4 \rightarrow YCrO_3 + 1/2O_2$. This reaction is fully completed between

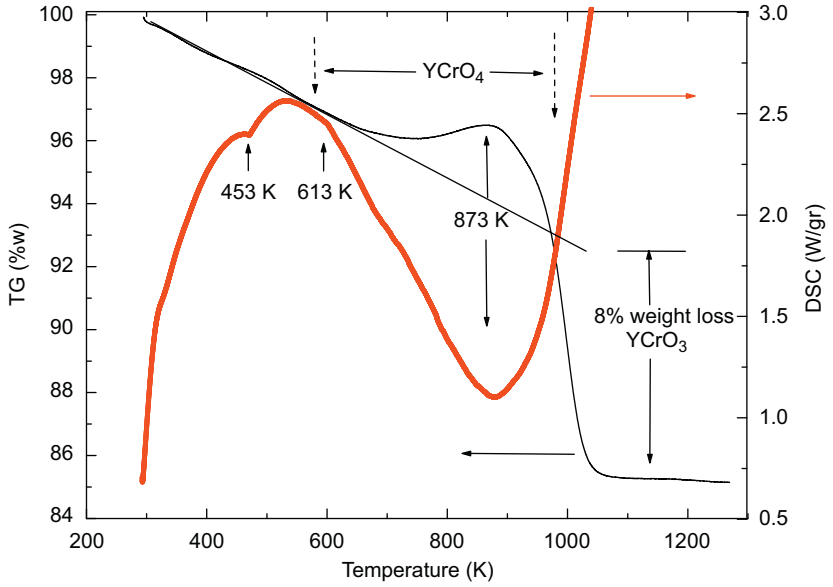

Fig. 1. DSC and TG curves for the combustion powder. The arrows indicate the range of the physicochemical changes upon heating: dehydration (85–180 °C), decomposition of the weakly coordinated precursors and releases of C, N and O in gaseous products (180–340 °C), crystallization of the first stable phase, $YCrO_4$ (400–700 °C), and finally the decomposition of the $YCrO_4$ toward the more stable $YCrO_3$ compound.

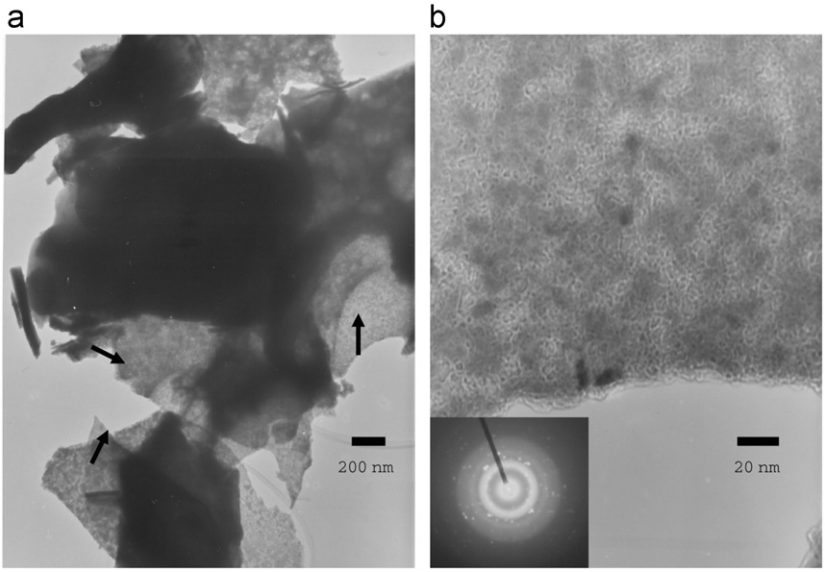

Fig. 2. TEM photographs for the combustion powder at (a) ×20 K and (b) ×250 K. The arrows indicate the overlap of conglomerated plates. The inset shows diffraction pattern of the plates.

~973 and ~1093 K with a weight loss of about 8%. This value is closed to the theoretical value of 7.81% corresponding to the loss of $1/2O_2$ per $YCrO_4$ mol.

Morphologic features, particles size and crystallinity of the as-prepared powder sample (after ignition) are observed by TEM images (Fig. 2a and b). At a magnification of ×20 K, Fig. 2a shows several different size plates with irregular morphology that overlap on the top each other (indicated by arrows). An inspection at higher magnification (×250 K) shows that the plates are formed by a conglomerate of nanoparticles of few nanometers as it is displayed in Fig. 2b. In addition, the nanoparticles are pseudo-crystalline as it is inferred from the discrete diffraction spots that are seen in the electron diffraction patterns (inset Fig. 2b). Apart from the crystalline nanoparticles, a less crystalline matrix is responsible for the appearance of diffuse rings in the diffraction pattern.

X-ray diffraction patterns which belong to the combustion product as well as the ball milled and fired powder at 1100 °C for 6 h are shown in Fig. 3a and b. The pattern confirms that the reaction products after the ignition are almost amorphous particles as it is seen by the absence of sharp diffraction peaks; however, several broad peaks corresponding to the main reflections of the orthochromite $YCrO_3$ as are seen at 2θ values of 32.7°, 43° and 49° in Fig. 3a. The crystalline phase is quickly obtained when the sample is fired at 1100 °C as it is observed in the fitted X-ray diffraction pattern (Fig. 3b). An excellent Rietveld fit profile at 295 K was obtained with an orthorhombic symmetry (S.G. *Pnma*) and there was no evidence of any distortion that suggests a non-centrosymmetric structure. The refined lattice parameters are as follows: $a=5.5239(7)$ Å, $b=7.5363(8)$ Å and $c=5.2438(7)$ Å, which are in good agreement with those reported in the literature [1,7,15].

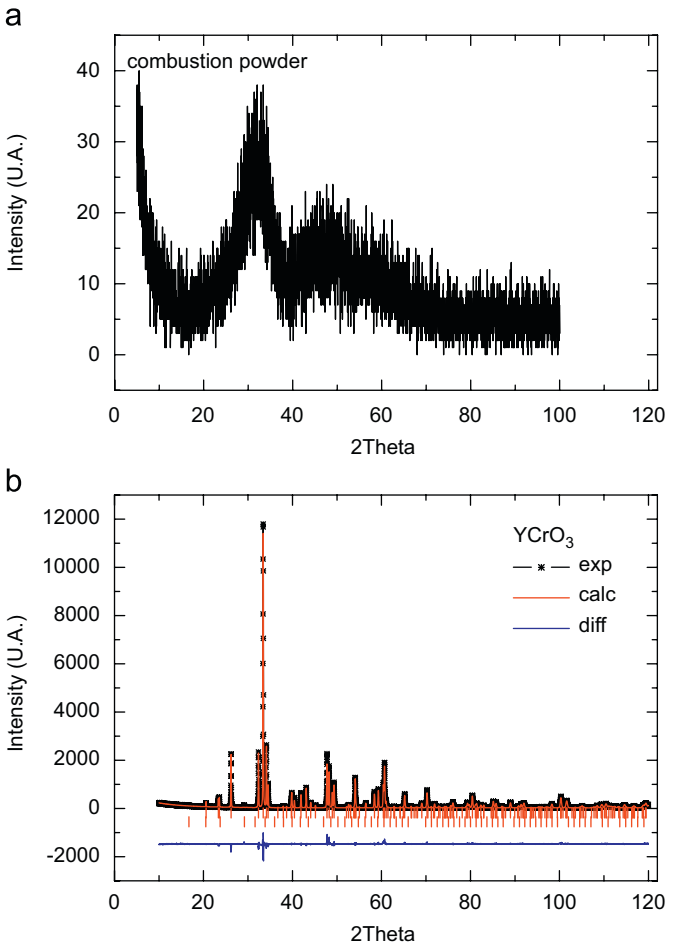

Fig. 3. X-ray diffraction spectra at 290 K for (a) the powder after ignition and (b) crystallized powder after firing at 1100 °C in $YCrO_3$. Refinement indicates that the calculated and experimental profile give a good goodness-of-fit (R_{wp}=9.10% and χ^2=1.6%).

The second phase included in the refinement (Y_2O_3) is present only after the first thermal treatment, but it disappears after subsequent thermal treatments.

Fig. 4 shows the SEM images after sintering of the products of the combustion and solid state reaction syntheses. For instance, it can be observed that the combustion route gave a more homogeneous grain size distribution (Figs. 4a and b), whereas different grain sizes are observed in the sample obtained through the solid state route (Figs. 4c and d). At higher magnification, it is evident that the sintering between particles is more uniform in the products of the combustion synthesis (Fig. 4b); it is also evident the heterogeneous morphology and grain size for materials obtained through a solid state route (Fig. 4d). The relative density calculated from volume and weight measurements on the pellets was about 65% and ~80% of the theoretical density, 5.742 g cm^{-3}, calculated from X-ray diffraction data, for the solid state reaction and combustion routes, respectively. The uniform size of the sintered particles in some way reduces the amount of pores and consequently increases the relative density of the material prepared through combustion synthesis with respect to that of products from solid state reaction process.

3.2. Magnetic and specific heat analysis

The temperature dependence of the susceptibility with applied magnetic fields of 0.1 and 10 kOe at $2 < T < 300$ K for the $YCrO_3$ powder obtained by the combustion route is shown in Fig. 5a. In the whole range of temperature, the magnetization rises as the magnetic field increases. Furthermore, a splitting in the ZFC and FC magnetization is seen at about 140 K which becomes larger at low applied magnetic fields leading to saturation in the FC mode at about 0.036 μ_B/f.u. for an external field of 10 kOe. This has been attributed to the transition of the Cr sublattice from a paramagnetic to a canted antiferromagnetic order (T_N) at low temperature being the splitting of the ZFC and FC mode due to the weak ferromagnetic ordering [6]. The inverse of susceptibility, $\chi-1$ versus temperature at 10 kOe is shown in the inset of Fig. 5a. The data follow the Curie–Weiss behavior for $T > 160$ K, according to

$$\chi = C/(T-\theta) = N_A\mu_{eff}^2/3k_B(T-\theta) \quad (1)$$

where C is the Curie constant, θ is the Weiss temperature, N_A is Avogadro's number, k_B is the Boltzmann constant and μ_{eff} is the effective magnetic moment per unit formula. Fitting the equation to the experimental data (continuous red line) it yields a value of μ_{eff}=3.77 μ_B. This value is closed to the theoretical value of μ_{eff}=3.87 μ_B for Hund's rule ground state of the Cr^{+3} when the orbital moments are quenched due to the crystalline electric field (CEF) effects as expected for a d^3 ion in octahedral environment. The Weiss temperature θ_W is found to be about −325 K, which is in agreement with antiferromagnetic interactions. On the other hand, a typical magnetization, M, versus applied magnetic field, H, at 5 K is shown in Fig. 5b. The hysteretic loop confirms the canted antiferromagnetic behavior where the anti-parallel spins have a magnetization different to zero. Furthermore, the high coercive field (~1.1 kOe) and the remanent magnetization (0.028 μ_B/f.u) are indicative of a not so weak ferromagnetic component. These magnetic properties are in agreement with those reported by Serrao et al. [5]. For the material prepared through solid state route and with those obtained for the nanopowders prepared through combustion synthesis does not influence the magnetic properties of the final material.

The magnetic ordering is also confirmed by specific heat measurements. Fig. 6a shows the total specific heat and the lattice contribution from 2 to 270 K. At room temperature, the molar specific heat reaches ~101 J/mol K that correspond to the ~80% of the Dulong–Petit equipartition value for five atoms ($C_p \sim 3NR$). At lower temperatures, a continuous λ-type anomaly is observed at ~140 K, typical behavior of a second order phase transition. This anomaly is associated with the canted antiferromagnetic ordering (T_N), in agreement with the magnetic transition observed in magnetization measurements previously discussed. In order to estimate the magnetic entropy near of T_N, first the phonon contribution is subtracted from the total specific heat. For this purpose, we use the Debye formula to calculate the lattice specific heat, in accordance with

$$C_{lat} = 9RN\left(\frac{T}{\Theta_D}\right)^3 \int_0^{\Theta/T} \frac{X^4 e^x}{(e^x-1)^2}\,dx \quad (2)$$

where N=5 is the number of atoms in the unit cell, R=8.314 J/mol K is the ideal gas constant and Θ_D is the Debye temperature. We chose Θ_D=720 so that the calculated C_{lat} coincides with the experimental value of C_p at high temperature (above 200 K). This approximation of the calculated data of C_{lat} is shown by the open circles in Fig. 6a. The magnetic contribution to the total C_p arises from the ordering of the Cr spins at T_N. It can be obtained by subtracting the lattice contribution to the total specific heat data, $C_{mag}=C_p-C_{lat}$, and it is plotted as C_{mag}/T in Fig. 6b. Thus, from this data the magnetic entropy is calculated by the numerical integration of C_{mag}/T from 5 to 270 K as it is seen by the solid line in Fig. 6b. The magnetic entropy (Δ_{mag}) at T_N is about 17.5 J/mol K. The obtained ΔS_{mag} value at T_N is larger than the expected theoretical value of ~11.526 J/mol K taking into account

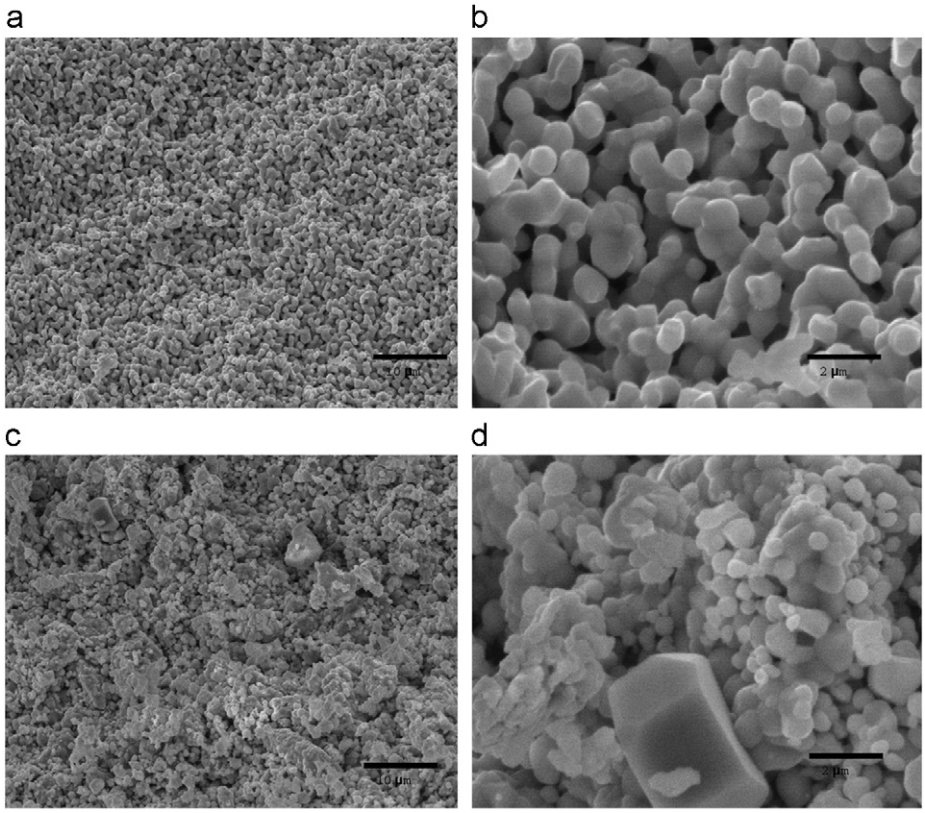

Fig. 4. (a, b) SEM photographs of $YCrO_3$ after the sintering process for materials obtained by the combustion method. (c, d) SEM images for sintered sample prepared by the solid state route.

that $\Delta S_{mag}=R\ln(2S+1)$ and $S=3/2$ for Cr^{+3}. It is interesting to note that the saturation of the magnetic entropy occurs at a temperature higher than that of the magnetic ordering, with a further residual magnetic gain to a total of 20.5 J/mol K at 270 K. The observation of this large excess of entropy at $T>T_N$ implies the existence of an additional spin entropy beyond the ground state of the magnetic entropy for Cr^{+3} ($S=3/2$). This also implies that part of the spin moment seems to be fluctuating leading quite likely to the development of a short-range order above T_N. In the χ^{-1} versus T plot, the magnetic fluctuation is manifested by slight deviation of the Curie–Weiss behavior above T_N ($T_N\sim140$ K). In conventional antiferromagnets the spin entropy takes constant values above T_N and magnon contributions only survive at low temperature (Ref. [16] and references therein). It is worthwhile noting that the magnetic contribution has a large residual weight showed as a broad peak at around 60 K in the C_{mag}/T plot. A similar behavior has been observed in frustrated manganites where the excess of the magnetic contribution to the specific heat below T_N has been attributed to spin fluctuations as a consequence of geometrical frustration existing in the internal Mn^{+3} triangular sublattice [16,17]. However, this does not seem the case of $YCrO_3$ compound. One plausible explanation could be associated to a spin reorientation mechanism. It is well known that some orthochoromites and (Pb, Bi)CrO_3 compounds display field/temperature induced spin reorientation [1,18–20]. At high temperature the configuration of the Cr magnetic lattice is determined by the crystalline anisotropy, and in $YCrO_3$ the antiferromagnetic easy axis lays along the x-axis [21]. We believe that the in absence of magnetic field the perpendicular spontaneous weak moment due to the antiferromagnetic spin canting rotates as the temperature is lowered. This behavior is seen, for the first time, by specific heat measurements from T_N to $\sim$60 K in Fig. 6b. The interaction between the Cr and Y cations becomes important and it is possible that around 60 K the antiferromagnetic easy x-axis results in a smooth rotation of the AFM-vector in the x–z plane as it was observed by Jacobs et al. [21]. In magnetic, ferroelectric and superconducting materials low lying modes contribute significantly to the low temperature specific heat which should be evident as a broad peak in the C_p/T^3 versus T plot [22–25]. This behavior is also seen in Fig. 6(c), where C_p/T^3 is plotted as a function of temperature for $YCrO_3$. There, a clear peak is seen around 40 K. Here, the excess of residual weight in C_{mag}/T data could indicate the development of magnon excitations as an optical phonon or even optical phonon softening as a consequence of the local non-centrosymmetric structure that occurs at about 450 K, as it will be seen in what follows.

3.3. Dielectric properties

The temperature dependence of the dielectric constant, ε' and loss tangent, tan δ for $YCrO_3$ synthesized by combustion method and solid state reaction are shown in Fig. 7a and b, respectively, with a comparison of the permittivity results from both samples in Fig. 7c. In both samples a broad peak is clearly seen at about 450 K. The dependence of the peak maxima with the frequency indicates a diffuse phase transition (DPT) rather than a classic ferroelectric to paraelectric phase transition. The $YCrO_3$ samples show a strong frequency dependence of both the dielectric constant and loss tangent being more notorious at low frequencies. The peak, at about 450 K, is smeared out at high frequencies. Furthermore, the behavior of the transition around 450 K is that typical of a relaxor material where the magnitude of the dielectric constant decreases with the increase of the frequencies at the same time that the maximum is shifted to higher temperatures [26,27]. It is known that relaxor materials are highly inhomogeneous materials in which a DPT arises due to

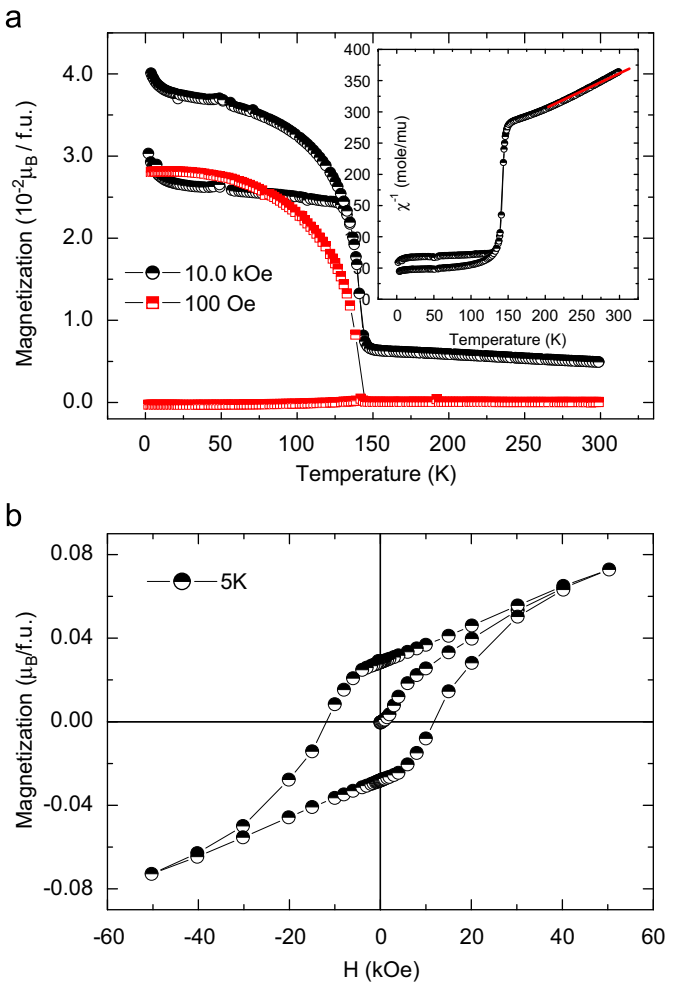

Fig. 5. (a) Magnetization as a function of temperature with external magnetic field of 0.1 and 10 kOe in ZFC and FC mode. The inset shows the inverse of the magnetic susceptibility as a function of temperature. The solid line is the fitted data between 200 and 300 K. (b) The external magnetic field dependence of the magnetization at 5 K for $YCrO_3$ prepared by the combustion method.

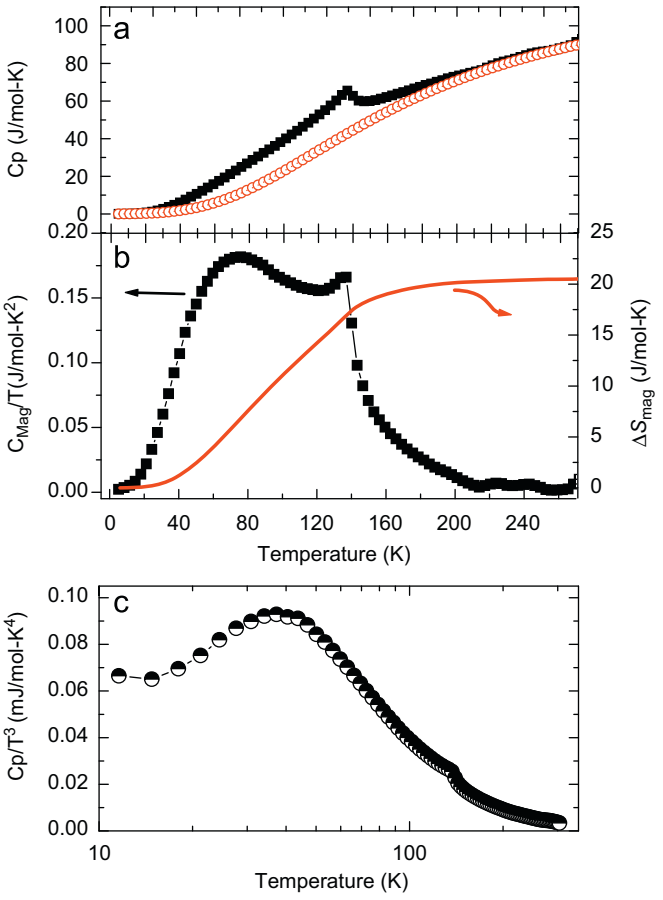

Fig. 6. (a) Total specific heat (black square) and lattice contribution to the specific heat as a function of temperature evaluated using the Debye formula (red circles). (b) The magnetic contribution to the specific heat, C_{Mag}/T (black squares) and the magnetic entropy contribution, ΔS_{mag} (continuous red line) as a function of temperature, (c) C_p/T^3 versus T curve for $YCrO_3$ combustion sample. (For interpretation of the references to color in this figure legend, the reader is referred to the web version of this article.)

a multitude of local phase transitions in a broad range of temperature [28], as it is shown in $YCrO_3$ material. Also, note that the magnitude of the dielectric constant at ~450 K in the sample obtained by the combustion method is about one order of magnitude higher than the one in the samples obtained by the solid state reaction as is seen in Fig. 7c, which we believe is due to the more homogeneous and lower particle size in combustion method with respect to the conventional method.

To describe the temperature dependence of the dielectric permittivity in the vicinity of the diffused phase transition, the following empirical power relation can be used:

$$\frac{1}{\varepsilon'}-\frac{1}{\varepsilon'_m}=\frac{(T-T_m)^{\alpha}}{C} \tag{3}$$

where ε'_m and T_m are the value and temperature of the $\varepsilon'(T)$ maximum value ε'_m corresponding to the phase transition for each frequency, C is the temperature independent coefficient and α is the diffuseness exponent indicative of the degree of disorder in the ferroelectric–paraelectric phase. The limiting values, from $1<\alpha<2$, reduce Eq. (3) to the Curie–Weiss law valid for a normal ferroelectric behavior at $\alpha=1$ and to the quadratic expression which is valid for a relaxor behavior at $\alpha=2$ [29]. The plots of ln $(1/\varepsilon'-1/\varepsilon'_m)$ versus ln $(T-T_m)$ at several frequencies are shown in Fig. 8. Fitting the $\varepsilon'(T)$ dependence in the paraelectric state (from ~470 to 550 K) gave a value of $\alpha=1.88$ and 1.98 for the sample synthesized for combustion and solid state reaction method, respectively. In both cases, a DPT is confirmed since the corresponding value of α is close to 2. Thus, the broadened peak and the deviation of the Curie–Weiss law can be ascribed to disorder caused intrinsically by a local non-centrosymmetric structure as were proposed by Ramesha et al. [8]. Small and well distributed grain size obtained through the combustion synthesis likely increases the local non-centrosymmetric nano-regions.

In order to know the conduction mechanism and the associated activation energy values, E_{act}, in $YCrO_3$ we have fitted the ac conductivity to an Arrhenius law as

$$\sigma(T)=\sigma_o e^{-(E_{act}/k_B T)} \tag{4}$$

where σ_o is the characteristic permittivity of the material, in general dependent of the frequency, k_B is the Boltzmann's constant, T is the absolute temperature and E_{act} is the activation energy associated with the conduction mechanism in the temperature region of temperature analyzed. The ln σ versus $1000/T$ is shown in Fig. 9, where the E_{act} can be calculated from the slope of the plot. The graph shows a region characterized by only one slope indicating the presence of one conduction mechanism. Thus, the activation Energy values are 0.38 and 0.32 eV for the products of the combustion and solid state reaction, respectively. The values of E_{act} are in correspondence with the hopping of charges, which should be associated to the incomplete outer d-shell in Cr+3 ($S=3/2$). This obtained value

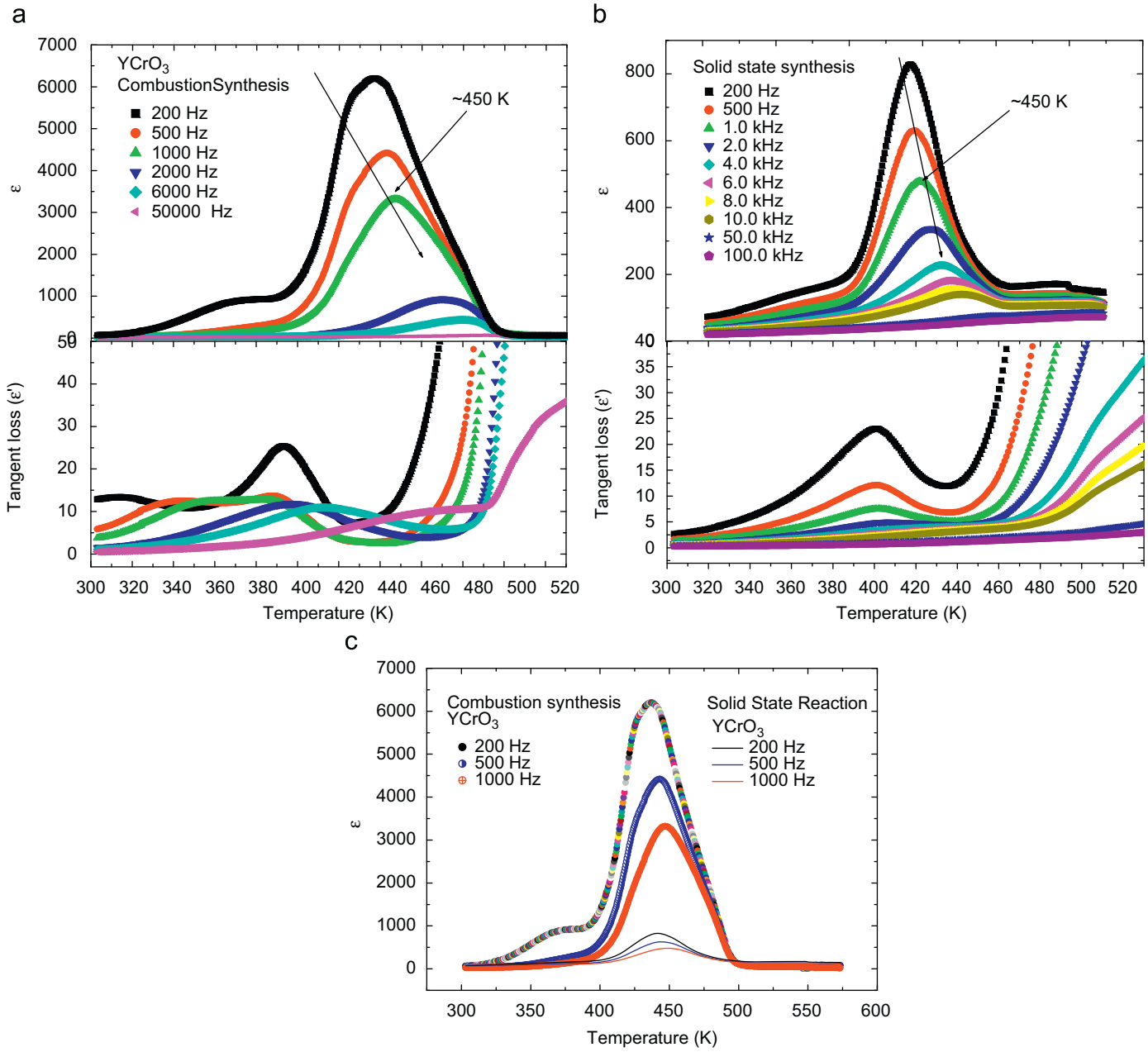

Fig. 7. (a, b) Dielectric constant and dielectric loss as a function of temperature at several frequencies for the combustion and solid state reaction for the $YCrO_3$ samples. (c) Compared dielectric constant curves as a function of temperature at 200, 500 and 1000 Hz for combustion and solid state $YCrO_3$ bulk samples.

corresponds to that reported for orthorhombic $FeNbO_4$ ([30] and references therein). Also, the average (E_{act}–0.35) in $YCrO_3$ are in correspondence to the extrinsic conductivity associated to small polarons (E_{act}~0.21–0.8) [30]. The result also shows that the combustion synthesis enhances the potential energy which stop the conductive process. This is likely due to the better grain homogenization and the low porosity obtained by combustion synthesis. Intergrain boundary in bulk ceramics plays an important role in the dielectric properties of the materials as it is seen in multiferroic $BiFeO_3$ [31]. In single crystal and thin films $BiFeO_3$ show a well defined hysteresis loops whereas in bulk ceramic the hysteresis loops are screened by the conductive process. In this case, the polarization measurements (not show here) displayed a circular-like hysteresis loop typical feature of a conductive process in bulk samples. This fact reveals that several conduction mechanisms are present as an intrinsic feature in the $YCrO_3$ samples. These conductive mechanisms give rise to leakage currents, which interfere with the polarization switching and pooling process.

4. Conclusions

Polycrystalline biferroic $YCrO_3$ was synthesized by the self-ignition process with a short calcinations step at relatively low temperatures in the successive sintering process. Uniform grain size, better control of the porosity and an increase of relative density is found in the samples obtained by the combustion method with respect to those prepared by long time high temperature solid state methods. The refined X-ray diffraction data did not show any signal of a structural distortion that could suggests a non-centrosymmetric crystal structure and the global S.G. *Pbnm* typical of an orthorhombic perovskite structure was observed. The magnetic properties do not seem to be influenced

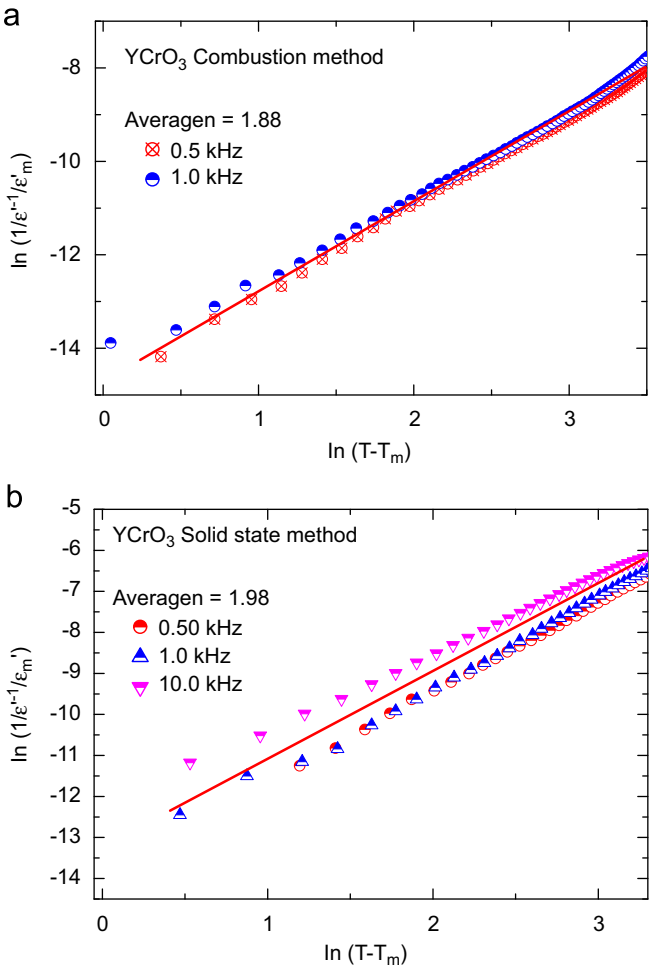

Fig. 8. ln $(1/\varepsilon'-1/\varepsilon'_m)$ versus $(T-T_m)$ temperature at several frequencies at higher than T_m for the $YCrO_3$ prepared by combustion and solid state reaction.

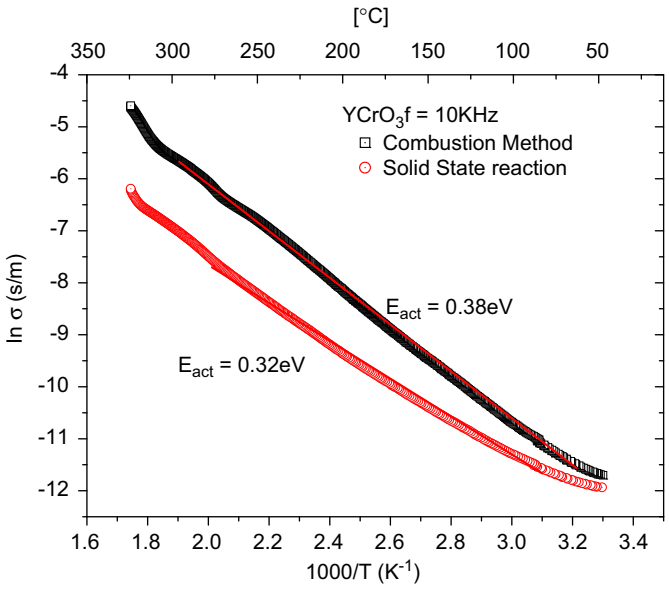

Fig. 9. Temperature dependence of ac conductivity at frequency of 10 kHz for combustion and solid state reaction method.

by the method of synthesis. At low temperatures, the magnetization and specific heat data show the typical second order phase transition from paramagnetic to a canted antiferromagnetic ordering at $T_N \sim 140$ K. A large excess of magnetic entropy indicates the development of short-range order at $T > T_N$ and in the absence of an external magnetic field, a spin reorientation takes place between T_N and ~ 60 K, that is observed as a broad peak in the C_p/T versus T plot. On the other hand, the dielectric properties and conduction mechanism are greatly influenced by the synthesis route and the thermal history of the material. The dielectric constant shows a broad peak at around 450 K with the magnitude and the maximum in temperature being notably dependent on frequency as typically occurs with relaxor materials. Moreover the material obtained through combustion method shows a stronger signal transition. The broadened peak and the large deviation of the Curie–Weiss law are associated to disorder intrinsically caused by grade of local non-centrosymmetric structure. Furthermore, the high tangent loss in a broad range of temperature is an indicative that the conductive mechanisms are present in $YCrO_3$. The conduction mechanism corresponds to the n- or p-type hopping of charges. In summary, we can state that the different combustion and solid state routes [6] have no effect on the Néel transition, T_N and hysteresis magnetization values; contrary to this fact, the synthesis route can be chosen to affect the magnitude of the DPT at ~ 450 K, as well as the conductive processes in $YCrO_3$.

Acknowledgments

A. D. thanks to CONACyT and DGAPA-UNAM through Project nos. 90562 and IN112909-3. M.P. C. thanks to DGAPA-UNAM through project IN107708-3. We also thank to S. Cardeña by computational data and E. Matesanz (UCM), J. Romero (UCM), J.M. Gallardo Amores (UCM), M. Canseco (IIM-UNAM), I. Gradilla (CNyN), E. Aparicio (CNyN), J. Palomares (CNYN) and P. Casillas (CNyN) for their technical help.

References

[1] J.B. Goodenough, W. Gräper, F. Holtzberg, D.H. Huber, R.A. Lefever, J.M. Longo, T.R. McGuire, S. Methfessel, in: Landolt-Börnstein—Band 4: Magnetische And Andere Eigenschaften Von Oxide Und Verwandten Verbindungen, Springer-Verlag, Berlin, Heidelberg, New York, 1970.
[2] V.M. Yudin, A.B. Sherman, Solid State Commun. 4 (1966) 661.
[3] E.F. Bertaut, J. Mareschal, Solid State Commun. 5 (1967) 93;
E.F. Bertaut, J. Mareschal, R. Pauthenet, J.P. Rebouillat, Bull. Soc. Fr. Ceram 43 (1966).
[4] A. DeCombarieu, A.J. Mareschal, J.C. Michel, J. Sivardiere, Solid State Commun. 6 (1968) 257;
R.M. Hornreich, S. Shtrikman, B.M. Wanklin, I. Yaeger, Phys. Rev. B 13 (1976) 4046;
T. Morishita, K. Tsushima, Phys. Rev. 24 (1981) 341.
[5] C.R. Serrao, A.K. Kundu, S.B. Krupanidhi, U.V. Waghmare, C.N.R. Rao, Phys. Rev. B 72 (2005) 220101(R).
[6] J.R. Sahu, C.R. Serrao, N. Ray, U.V. Waghmare, C.N.R. Rao, J. Mater. Chem. 17 (2007) 42.
[7] S. Geller, E.A. Good, Acta Crystallogr. 1 (1967) 948;
S. Quezel-Ambrunaz, M. Mareschal, Bull. Soc. Fr. Miner. Crystallogr. 86 (1963) 204.
[8] K. Ramesha, A. Llobet, Th Proffen, C.R. Serrao, C.N.R. Rao, J. Phys.: Condens. Matter 19 (2007) 102202.
[9] K.C. Patil, S.T. Aruna, T. Mimani, Curr. Opin. Solid State Mater. Sci. 6 (2002) 507.
[10] L.E. Smart, Elaine A. Moore, in: Solid State Chem., third ed., Taylor & Francis Group, 2005;
B.I. Lee, E.J.A. Pope, in: Chemical Processing of Ceramic, Marcel Dekker Inc., 1994.
[11] B. Hunter, Rietica – A visual Rietveld program. International Union of Crystallography Commission on Powder Diffraction Newsletter No. 20, (Summer), 1998, http://www.rietica.org.
[12] V. Bedekar, R. Shukla, A.K. Tyagi, Nanotechnology 18 (2007) 155706.
[13] T. Tachiwaki, Y. Kunifusa, M. Yoshinaka, K. Hirota, O. Yamaguchi, Int. J. Inorg. Mater. 3 (2001) 107.
[14] S. Wang, B. Lin, Y. Dong, D. Fang, H. Ding, X. Liu, G. Meng, J. Power Source 188 (2009) 48.

[15] S. Geller, E.A. Wood, Acta Crystallogr. 9 (1956) 563.
[16] H.D. Zhou, J.A. Janik, B.W. Vogt, Y.J. Jo, L. Balicas, M.J. Case, C.R. Wiebe, J.C. Denyszyn, J.B. Goodenough, J.G. Cheng, Phys. Rev. B 74 (2006) 094426.
[17] T. Katsufuji, S. Mori, M. Masaki, Y. Moritomo, N. Yamamoto, H. Takagi, Phys. Rev. B 64 (2001) 104419.
[18] A.H. Cooke, D.M. Martin, M.R. Wells, J. Phys. C: Solid State Phys. 7 (1974) 3133.
[19] A.M. Arévalo-López, A.J. Dos santos-García, M. Alario-Franco, Inorg. Chem. 48 (2009) 5434.
[20] A.A. Belik, N. Tsujii, H. Suzuki, E. Takayama-Murumachi, Inorg. Chem. 46 (2007) 8746.
[21] I.S. Jacobs, H.F. Burne, L.M. Levinson, J. Appl. Phys. 42 (1971) 1631.
[22] W.L. Lawless, Phys. Rev. B 14 (1976) 134.
[23] W.N. Lawless, Phys. Rev. B 18 (1978) 2394.
[24] M. Tachibana, J. Yamazaki, H. Kawaji, T. Atake, Phys. Rev. B 72 (2005) 064434.
[25] A. Durán, F. Morales, L. Fuentes, J.M. Siqueiros, J. Phys.: Dens. Matter 20 (2008) 085219.
[26] C. Randall, A. Bhalla, T. Shrout, L.E. Cross, J. Mater. Res. 5 (1990) 829.
[27] L.E. Cross, Ferrolectrics 76 (1987) 241.
[28] D. Viehland, S.J. Jang, L.E. Cross, J. Appl. Phys. 68 (1990) 2916.
[29] G.A. Smolebsky, J. Phys. Soc. Jpn. 28 (1970) 26.
[30] O. Raymond, R. Font, N. Suarez-Almodovar, J. Potelles, J.M. Siqueiros, J. Appl. Phys. 97 (2005) 08407.
[31] G. Catalan, J.F. Scott, Adv. Mater. 21 (2009) 2463.